Ferromagnetic Shape Memory in the NiMnGa System

R. Tickle, R. D. James, T. Shield, M. Wuttig, and V. V. Kokorin

Abstract—**Strain versus field measurements for a ferromagnetic shape memory alloy in the NiMnGa system demonstrate the *largest magnetostrictive strains to date of nearly 1.3%. These* strains are achieved in the martensitic state through field-induced variant rearrangement. An experimental apparatus is described that provides biaxial magnetic fields and uniaxial compressive prestress with temperature control while recording microstructural changes with optical microscopy. The magnetostrictive response is found to be sensitive to the initial state induced by stress-biasing the martensitic variant structure, and exhibits rate effects related to twin boundary mobility. Experiments performed with constant stress demonstrate work output capacity. Experimental results are interpreted by using a theory based on minimization of a micromagnetic energy functional that includes applied field, stress, and demagnetization energies. It is found that the theory provides a good qualitative description of material behavior, but significantly overpredicts the amount of strain produced. Issues concerning the martensitic magnetic anisotropy and variant nucleation are discussed with regard to this discrepancy.**

Index Terms— **Cubic-to-tetragonal transformation, ferromagnetic shape memory, giant magnetostrictive materials, magnetomechanical properties.**

I. Introduction

FERROMAGNETIC shape memory refers to the reversible change of shape of a martensitic material caused by either rearranging the variants of martensite or by inducing the austenite/martensite transformation with an applied magnetic field. The conditions on material constants and transformation parameters that promote this effect have been studied by James and Wuttig [1], [2] and a "constrained" theory of magnetostriction intended to describe strain versus field and the associated microstructural changes in these materials is given by DeSimone and James [3].

In this paper we study ferromagnetic shape memory, particularly the rearrangement of martensitic variants by an applied field, in Ni_2MnGa. Our main observations are field-induced strains of about 0.5% during cyclic application of the magnetic field below the austenite/martensite transformation temperature, and strains of 1.3% upon application of a field from a stress-biased state at similar temperatures. Observations of microstructure confirm that these changes of shape are caused by the field-induced rearrangement of martensite variants. The variant redistribution is produced by fields under 10 000 Oe at temperatures around −15 °C. The strains reported here are 5–10 times larger than those observed in the giant magnetostrictive material $Tb_{0.3}Dy_{0.7}Fe_2$. We report the results of three different tests suggested by the theory as favorable for producing large field-induced changes of shape under moderate field. The general strategy of the tests was to use a uniaxial magnetic field or compressive stress to bias a certain domain structure, and then apply a competing variable magnetic field to induce the change of shape.

Field-induced changes of shape in the NiMnGa system were reported by Ullakko *et al.* [4]. They demonstrated reversible field-induced strains of about 0.2% under cyclic fields of 10 000 Oe applied parallel to a rod along [001]. James and Wuttig [1] showed cyclic field-induced strains of 0.5% in $Fe_{70}Pd_{30}$ using a preliminary version of the present apparatus. These experiments are contrasted with the present results in the final section.

Recently, O'Handley [5] has given a model for the behavior of Ni_2MnGa and other magnetic shape memory alloys. This model, which is based on a particular twinned domain structure, shows good agreement with experiments of Ullakko *et al.* and accounts for magnetic anisotropy.

In Section II we describe in some detail the experimental apparatus and procedure used in the experiments studied here and in James and Wuttig [1]. Section III describes the micromagnetic theory used to predict the behavior of shape memory ferromagnets. This theory assumes that, except possibly on narrow transition layers, the magnetization lies on certain specific easy axes of the martensite variants. This corresponds to the ideal case described by James and Wuttig in which the easy axes are essentially fixed to the lattice and an applied field causes a redistribution of martensite variants. The theory allows all possible compatible arrangements of martensite variants to compete for the minimum of the free energy, and therefore can be used effectively to assess its hypotheses. In Section IV we apply the theory to the three experiments performed to obtain predictions of strain versus field and the associated microstructures. The theory shows good qualitative agreement with the three experiments, indicating strongly that the c axis is the easy axis of the martensite, but shows significant quantitative disagreement. This is discussed in Section V.

Manuscript received November 4, 1998; revised June 1, 1999. This work was supported by ONR/ARPA (RDJ & TWS: N00014-95-1-1145 and -91-J-4034; MW: N00014-95-11071 and -93-10506); the AFOSR (RDJ: 49620-96-1-0057), the ARO (MW: DAAL03-92-G-0121), and the NSF (MW: DMR-93-21185; RDJ: DMS-9505077).

R. Tickle, R. D. James, and T. Shield are with the Department of Aerospace Engineering and Mechanics, University of Minnesota, Minneapolis, MN 55455 USA (e-mail: tickle@aem.umn.edu).

M. Wuttig is with the Department of Materials and Nuclear Engineering, University of Maryland, College Park, MD 20742 USA.

V. V. Kokorin is with the Institute for Magnetism, 252680 Kiev, Ukraine.

Publisher Item Identifier S 0018-9464(99)07904-2.

II. Experimental Method

The specimen used for all experiments described was cut from a single crystal boule with composition $Ni_{51.3}Mn_{24.0}Ga_{24.7}$, as determined by a scanning electron microscope equipped with EDS. The specimen dimensions were 2 mm × 2 mm × 12 mm, and the boule was oriented using Laue X-ray diffraction to obtain {100} specimen faces. Strains were measured by a resistance strain gage bonded along the long axis ([100]) of the specimen. The martensitic transformation temperature M_s was determined both visually and with DSC measurements to be $M_s \approx -10$ °C, and the temperature hysteresis associated with the transformation was less than 3 °C. The Curie temperature T_c was determined with susceptibility measurements and found to be $T_c \approx 85$ °C, indicating that both austenitic and martensitic phases are ferromagnetic in this alloy. The saturation magnetization m_s of the martensitic phase was measured with a vibrating sample magnetometer equipped with a cooling chamber. At −15 °C, the value was determined to be $m_s = 602$ emu/cm^3.

The experimental apparatus was designed to perform three types of tests:

- fixed axial field, variable transverse field;
- fixed transverse field, variable axial field;
- fixed axial compressive stress, variable transverse field.

Here the axial direction refers to the long axis of the specimen. Fixed magnetic fields were produced with a pair of NdFeB magnets mounted on a support bar surrounding the specimen holder. The distance between these permanent magnets could be adjusted; in the tests reported here they were spaced to produce fixed fields of 2500 Oe and 3500 Oe. The support bar was mounted between the pole pieces of a 1.5 T Lakeshore electro-magnet which provided all variable fields for the tests. The uniformity of the fields produced by both the permanent magnets and the electromagnet was measured and found to be constant within ±5% across the length of the specimen.

In order to induce the martensitic transformation, a temperature controlled specimen holder was built which circulated cooled nitrogen gas to maintain a temperature of around −15 °C, as measured with a thermocouple attached to the holder. The specimen holder was centered on the support bar between the two permanent magnets and could be rotated to align the axial or transverse direction of the specimen with the static field. Compressive stress was applied to the specimen by a dowel pin in series with a small aluminum spring and measured with a load cell. The spring was designed to be extremely soft to accommodate the large strains associated with martensitic materials without a large change in applied load. The top face of the specimen was polished to allow *in situ* observations of martensite microstructure with differential interference contrast (DIC) or simple polarized light microscopy. The microscope used a nonmagnetic objective holder and was mounted between the coils of the electromagnet and equipped with video and still cameras. Figs. 1 and 2 show schematic illustrations of the experimental setup, as well as the coordinate system used for the analysis.

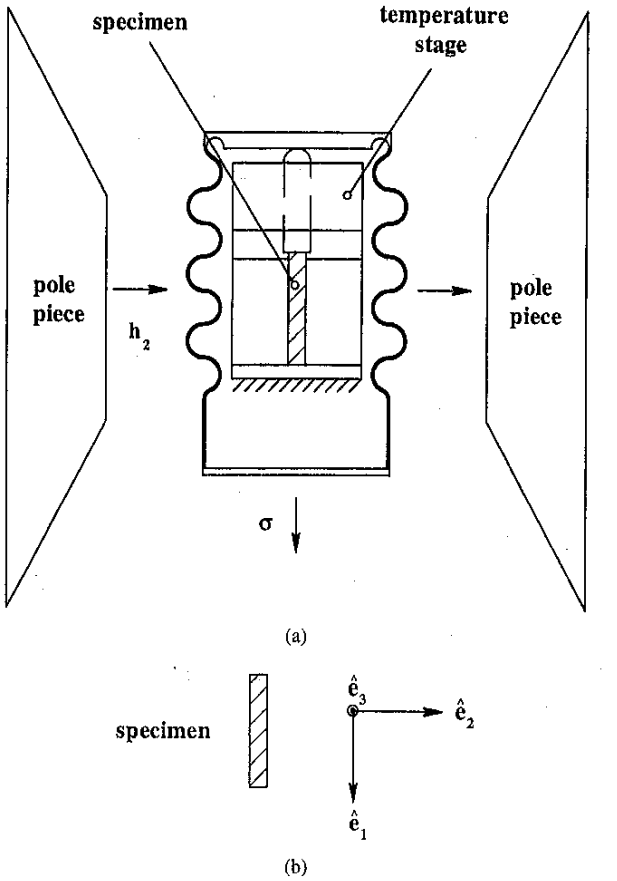

Fig. 1. (a) Fixed axial compression, variable transverse field experimental apparatus. (b) Experiment coordinate system used.

III. Micromagnetic Theory

Recently a theory has been developed to predict the evolution of microstructure in ideal ferromagnetic shape memory materials [3], [6]. The theory is based on the micromagnetic approach initially developed by Landau and Lifshitz [7] and later formalized by Brown [8]. In this approach, a suitable micromagnetic energy functional which includes the effects of applied fields and loads is minimized from within a "constrained" space of possible deformations and magnetizations. The conditions under which the constrained theory is valid are compatible with the existence of ferromagnetic shape memory; these conditions are discussed in detail elsewhere [1], [3], [6].

Specifically, the theory assumes that the martensitic material energetically prefers to experience a small set of deformations, associated with the variants of martensite, and that each variant has an associated magnetization. In the case of the cubic to tetragonal transformation found in Ni_2MnGa, there are three martensite variants. Each variant corresponds to the homogeneous deformation produced by contracting a cube along one of its edges and extending it along the other two. The easy axis of magnetization in each variant is assumed to point along the short axis. We represent variant i by its small strain tensor $\mathbf{E}_i$, where $\mathbf{E}$ is given by the usual formula in terms of the displacement gradient: $\mathbf{E} = 1/2(\nabla \mathbf{u} + (\nabla \mathbf{u})^T)$,

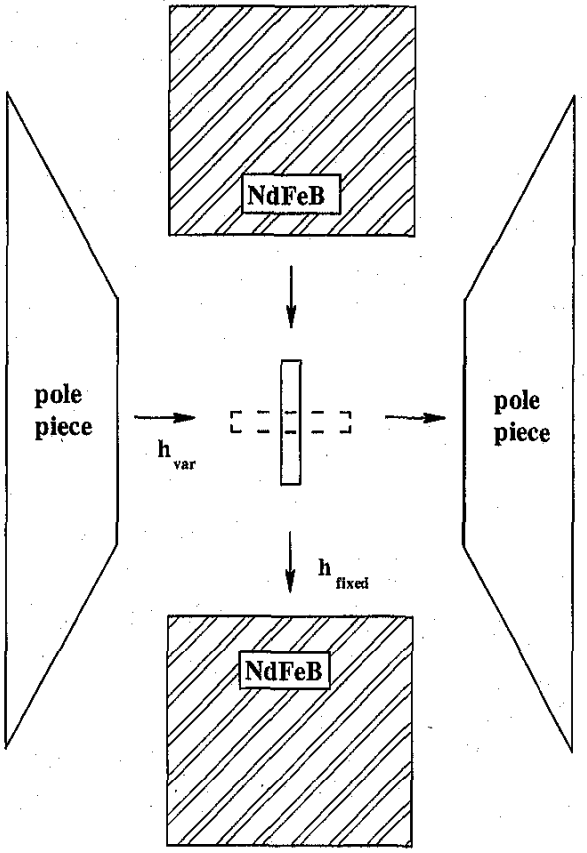

Fig. 2. Specimen orientations for fixed axial, variable transverse field (solid) and fixed transverse, variable axial field (dashed) experiments.

where T represents the transpose operator. We can then write the set of three variants with their associated magnetizations as

$$\mathbf{E}_1 = \begin{pmatrix} \epsilon_2 & & \\ & \epsilon_1 & \\ & & \epsilon_1 \end{pmatrix}, \mathbf{m}_1 = m_s(100)$$

$$\mathbf{E}_2 = \begin{pmatrix} \epsilon_1 & & \\ & \epsilon_2 & \\ & & \epsilon_1 \end{pmatrix}, \mathbf{m}_2 = m_s(010)$$

$$\mathbf{E}_3 = \begin{pmatrix} \epsilon_1 & & \\ & \epsilon_1 & \\ & & \epsilon_2 \end{pmatrix}, \mathbf{m}_3 = m_s(001) \qquad (1)$$

where m_s is the saturation magnetization of the martensite, and lattice parameter data from Zasimchuk *et al.* [9] for the alloy considered here indicates that $\epsilon_2 < 0 < \epsilon_1$.

Fig. 3 illustrates the three variants that arise on cooling below critical temperature M_s in the cubic-tetragonal phase transformation in Ni_2MnGa. The lattice deformations associated with each variant are shown with the strains exaggerated for clarity. Note that the points in these lattice examples indicate the deformations of the unit cell and are not intended to describe the full Heusler lattice structure. A typical martensitic microstructure consists of mixtures of the three variants in which two adjacent variants meet at one of two possible well-defined interfaces called twin planes.

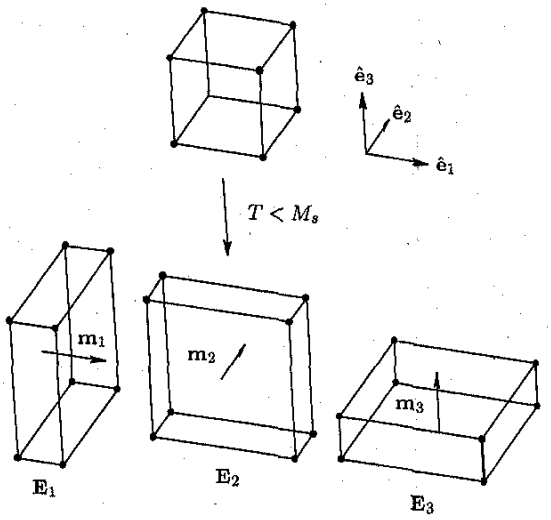

Fig. 3. Lattice deformations corresponding to the three variants of martensite. Strains exaggerated for clarity.

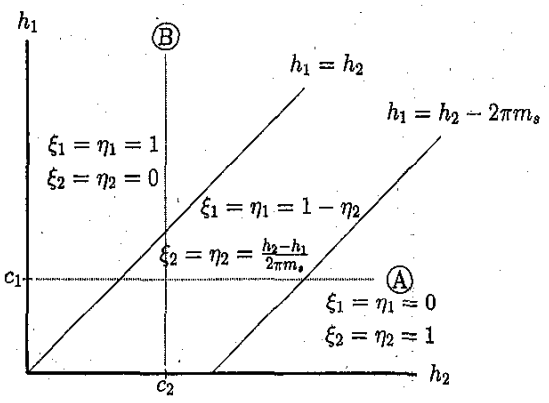

(a)

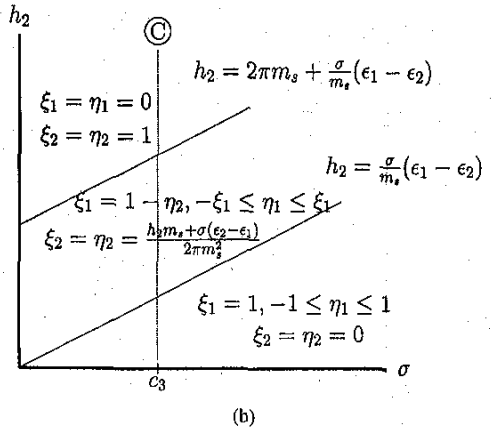

(b)

Fig. 4. Critical fields and solutions for (a) dual field and (b) stress-field experiments. Paths A, B, C correspond, respectively, to experiments analyzed in Sections IV-A, IV-B, and IV-C.

The energy minimizing states of the magnetoelastic energy density of the martensite are referred to as energy wells. In the constrained theory, deformations and magnetizations are

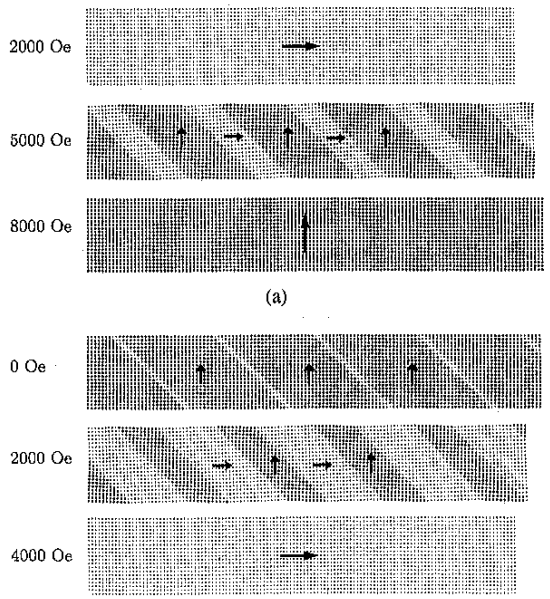

Fig. 5. Predicted energy minimizing magnetoelastic domain structures for (a) Fixed 2500 Oe axial field, variable transverse field and (b) Fixed 3500 Oe transverse field, variable axial field. Light dots: variant 1. Dark dots: variant 2.

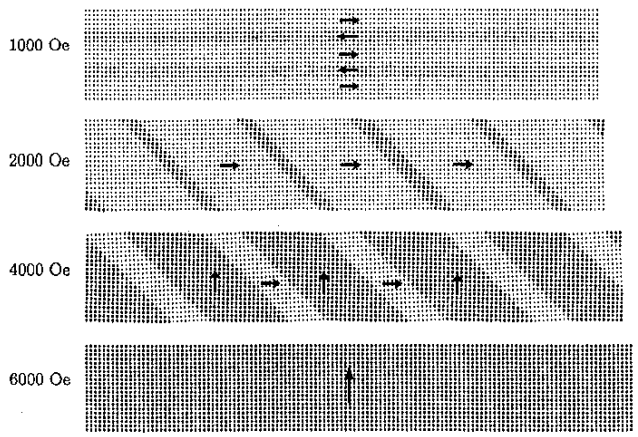

Fig. 6. Predicted energy minimizing magnetoelastic domain structures for 1.4 MPa axial compression, variable transverse field. Light dots: variant 1, magnetization $\mathbf{m}_1$. Dark dots: variant 2. Medium dots: variant 1, magnetization $-\mathbf{m}_1$.

restricted to the states given by strain-magnetization pairs $(\mathbf{E}_i, \pm\mathbf{m}_i)$. These pairs then represent the set of energy wells. Energy minimizing states are determined by

$$\min_{\substack{(\mathbf{E}(\mathbf{x}),\,\mathbf{m}(\mathbf{x}))\\ \in\text{wells}}} -\mathbf{h}_0\cdot\langle\mathbf{m}\rangle-\boldsymbol{\sigma}_0\cdot\langle\mathbf{E}\rangle+\frac{1}{8\pi}\int_{R^3}|\nabla\zeta_{\mathbf{m}}|^2\,d\mathbf{x}+\text{excess} \tag{2}$$

where

$$\langle\mathbf{m}\rangle=\frac{1}{\text{vol. }\Omega}\int_\Omega\mathbf{m}(\mathbf{x})\,d\mathbf{x},\quad \langle\mathbf{E}\rangle=\frac{1}{\text{vol. }\Omega}\int_\Omega\mathbf{E}(\mathbf{x})\,d\mathbf{x}$$

are the average strain and magnetization, and applied field $\mathbf{h}_0$ and stress $\boldsymbol{\sigma}_0$ are assumed to be constant. The integral term in (2) is the magnetostatic energy, where $\zeta_{\mathbf{m}}$ is the magnetostatic potential arising from Maxwell's equation $\nabla\times(-\nabla\zeta_{\mathbf{m}}+4\pi\mathbf{m})=0$, and the "excess" term represents positive energy contributed by the presence of internal poles. The term $-\boldsymbol{\sigma}_0\cdot\langle\mathbf{E}\rangle$ represents the energy of a dead load with stress $\boldsymbol{\sigma}_0$, to model the very soft loading device used in the experiments.

In order to simplify the energy expression (2), we first consider the pairwise compatibility of strain-magnetization pairs $(\mathbf{E}_i, \pm\mathbf{m}_i)$. Roughly speaking, the property of pairwise compatibility allows two variants to meet at a pair of well-defined twin boundaries, and the associated magnetizations to be divergence-free. For Ni_2MnGa, all $(\mathbf{E}_i, \pm\mathbf{m}_i)$ are pairwise compatible with each other [3]. In this case, it can be shown [3], [10] that the "excess" energy is zero, and the full set of average strain-magnetization pairs can be described by the convex hull $\mathcal{C}$ of $(\mathbf{E}_1, \pm\mathbf{m}_1)$, $(\mathbf{E}_2, \pm\mathbf{m}_2)$, $(\mathbf{E}_3, \pm\mathbf{m}_3)$, defined in the following way:

$$\begin{aligned}(\langle\mathbf{E}\rangle, \langle\mathbf{m}\rangle)\in\mathcal{C}\Leftrightarrow\\ \langle\mathbf{m}\rangle=&\lambda_1\mathbf{m}_1+\lambda_2(-\mathbf{m}_1)+\lambda_3\mathbf{m}_2+\lambda_4(-\mathbf{m}_2)\\ &+\lambda_5\mathbf{m}_3+\lambda_6(-\mathbf{m}_3)\\ \langle\mathbf{E}\rangle=&(\lambda_1+\lambda_2)\mathbf{E}_1+(\lambda_3+\lambda_4)\mathbf{E}_2+(\lambda_5+\lambda_6)\mathbf{E}_3\end{aligned} \tag{3}$$

where $0\le\lambda_i\le 1$ and $\sum\lambda_i=1$. The basic theory says that in the case of pairwise compatibility, any average strain-magnetization pair given by (3) can be produced by certain hierarchical laminates of the variants along with their associated magnetic substructures.

To further simplify (2), we make the assumption that Ω is an ellipsoid. Note that if we fix the average strain $\langle\mathbf{E}\rangle$ and average magnetization $\langle\mathbf{m}\rangle$, then minimization of (2) is equivalent to the minimization of the magnetostatic energy. For fixed average magnetization, and with Ω an ellipsoid, the magnetostatic energy is minimized by constant magnetization $\mathbf{m}(\mathbf{x})=\langle\mathbf{m}\rangle$. The value of the minimum is $(1/2)\langle\mathbf{m}\rangle\cdot\mathbf{D}\langle\mathbf{m}\rangle$ where $\mathbf{D}$ is the demagnetization matrix for the ellipsoid Ω. See DeSimone and James [3] for details of this calculation.

Using these simplifications, the minimization problem (2) is reduced to a quadratic programming problem

$$\min_{(\langle\mathbf{E}\rangle,\,\langle\mathbf{m}\rangle)\in\mathcal{C}}\left\{-\mathbf{h}_0\cdot\langle\mathbf{m}\rangle-\boldsymbol{\sigma}_0\cdot\langle\mathbf{E}\rangle+\tfrac{1}{2}\langle\mathbf{m}\rangle\cdot\mathbf{D}\langle\mathbf{m}\rangle\right\} \tag{4}$$

whose solution is a set of minimizing volume fractions $\lambda_1, \lambda_2, \ldots, \lambda_6$; from these the theory guarantees at least one compatible magnetoelastic domain structure. In general, these volume fractions are a function of the applied field and load, and they describe the evolution of the microstructure as fields and loads are changed.

In order to solve the minimization problem (4), it is helpful to make the substitution

$$\begin{aligned}\xi_1&=\lambda_1+\lambda_2, & \xi_2&=\lambda_3+\lambda_4, & \xi_3&=\lambda_5+\lambda_6\\ \eta_1&=\lambda_1-\lambda_2, & \eta_2&=\lambda_3-\lambda_4, & \eta_3&=\lambda_5-\lambda_6.\end{aligned}$$

Then the average strain and magnetization can be written as

$$\begin{aligned}\langle\mathbf{E}\rangle&=\xi_1\mathbf{E}_1+\xi_2\mathbf{E}_2+\xi_3\mathbf{E}_3\\ \langle\mathbf{m}\rangle&=\eta_1\mathbf{m}_1+\eta_2\mathbf{m}_2+\eta_3\mathbf{m}_3\end{aligned}$$

where ξ_i is the volume fraction of variant i, and η_i is the net magnetization associated with variant i. The constraints

$0 \le \lambda_i \le 1$ and $\Sigma\lambda_i = 1$ then become

$$\xi_i \ge |\eta_i|, \qquad \xi_1 + \xi_2 + \xi_3 = 1. \tag{5}$$

IV. Comparison of Theory and Experiment

We now apply the theory to the three experiments performed and compare with the results. We use the following orthonormal basis: $\hat{\mathbf{e}}_1$ denotes the specimen axial [100] direction, $\hat{\mathbf{e}}_2$ the transverse [010] direction, and $\hat{\mathbf{e}}_3$ the normal [001] direction [see Fig. 1(b)]. The demagnetization matrix $\mathbf{D}$ is taken to be that appropriate for an infinitely long rod with axis $\hat{\mathbf{e}}_1$. Then we can write

$$\mathbf{h}_0 = h_1\hat{\mathbf{e}}_1 + h_2\hat{\mathbf{e}}_2, \qquad \boldsymbol{\sigma}_0 = -\sigma\hat{\mathbf{e}}_1 \otimes \hat{\mathbf{e}}_1, \quad \sigma \ge 0$$
$$\mathbf{D} = \begin{pmatrix} 0 & & \\ & 2\pi & \\ & & 2\pi \end{pmatrix}. \tag{6}$$

For the dual field experiments, we set $\sigma = 0$ and substitute (6) into (4) to get

$$\min_{\xi_i,\eta_i \text{ satisfy (5)}} \left\{-h_1 m_s \eta_1 - h_2 m_s \eta_2 + \pi m_s^2\left(\eta_2^2 + \eta_3^2\right)\right\}. \tag{7}$$

In the case of the axial compression, transverse field experiment, we set $h_1 = 0$ and get

$$\min_{\xi_i,\eta_i \text{ satisfy (5)}} \left\{-h_2 m_s \eta_2 + \pi m_s^2\left(\eta_2^2 + \eta_3^2\right) + \sigma(\xi_1\epsilon_2 + (\xi_2 + \xi_3)\epsilon_1)\right\}. \tag{8}$$

For both cases, we set $\xi_3 = 0$; this condition corresponds to the absence of variant $\mathbf{E}_3$, whose easy axis and short axis is in the $\hat{\mathbf{e}}_3$ direction. In the dual field tests this seems reasonable since neither field favors this easy axis. In the axial compression tests we note that compression favors only variant $\mathbf{E}_1$, since this is the only variant whose short axis coincides with the compression axis, while the transverse field favors variant $\mathbf{E}_2$. By setting $\xi_3 = 0$ it follows from (5) that $\eta_3 = 0$ also. These two conditions simultaneously minimize the energy in both (7) and (8), while maximizing the size of the constraint set through (5).

The solution of (7) describes the evolution of net magnetizations η_1, η_2 in (h_1, h_2) space, and the corresponding values of ξ_1, ξ_2 are then uniquely determined from the constraints (5). Similarly, the solution of (8), together with the constraints (5), determines the minimizing values of η_1, η_2 and ξ_1, ξ_2 in (h_2, σ) space. As is typical of quadratic programming problems, the nature of the solution changes at critical values of the applied field or stress. It is found that the solution moves from multivariant to single variant states at certain critical fields determined by the parameters of the test (i.e., load or field) and by material constants m_s and ϵ_1, ϵ_2. Fig. 4 gives a summary of the predicted volume fractions and the critical fields. The dashed lines shown there correspond to the experimental tests that were conducted. Only the first quadrant of each solution space is shown; in all cases the solutions obtained from (7) and (8) are found to be symmetric with respect to the applied field, and one can assume without loss of generality that either the fixed fields or loads are positive. From any solution the axial strain can then be calculated using

$$|\langle\mathbf{E}\rangle\hat{\mathbf{e}}_1| = \epsilon_2\xi_1 + \epsilon_1(\xi_2 + \xi_3). \tag{9}$$

Lattice parameter data taken from [9] gives $\epsilon_1 \approx 0.013$, $\epsilon_2 \approx -0.048$, where ϵ_1, ϵ_2 are the strains associated with the long and short axes of the variants, respectively. The saturation magnetization m_s of the martensite was taken to be $m_s = 602$ emu/cm^3 for all experiments. Strain-field curves were constructed using this data and (9). One possible sequence of energy minimizing microstructures for each of the three tests is shown in Figs. 5(a) and (b), and 6. Two comments about these figures are in order: They are plotted using the real preferred strains ϵ_1 and ϵ_2, so the dimensions of the small squares are proportional to unit cell dimensions and the predicted macroscopic strains and microscopic rotations can be observed directly from the plots. Second, the layered microstructures shown should be much finer than specimen dimensions in keeping with the large body assumption used in the theory. We consider each experiment individually in the following sections.

A. Fixed Axial Field, Variable Transverse Field

Here we fix $h_1 = c_1 = 2500$ Oe, and cycle the transverse field h_2 about zero. For this experiment and all others (except the rate effect experiment described below), the variable field was ramped at a rate of 150 Oe/s. This test corresponds to path A in Fig. 4(a), where the fixed value c_1 of the axial field is noted on the h_1 scale. Fig. 7 shows the predicted strain-field curve and the experimental curve. Fig. 5(a) shows one possible series of compatible magnetoelastic domain structures corresponding to the predicted strain-field curve. In this sequence, the fixed axial field initially biases a single variant structure (variant one). As the transverse field is applied and overcomes demagnetization energy, variant two is introduced. Finally, at 8000 Oe, the microstructure is completely transformed to variant two.

The theory shows qualitative agreement with the measurement in terms of the form and symmetry of the curves but significant quantitative disagreement. The qualitative agreement (here and in the following two sections) indicates that the easy axes chosen in (1) are appropriate. These are quite different than those found to be appropriate in $Fe_{70}Pd_{30}$, which also undergoes a cubic-tetragonal transformation with $\epsilon_2 < 0 < \epsilon_1$. We note that if other low index easy axes are used in (1), then there is gross qualitative disagreement with experiment. The experimental curves also show a flat region where, according to the theory, the transverse field competes with both the axial field and with demagnetization effects.

It is important to note that the experimental curve shows no evidence of saturation in this case; with larger fields, it may be possible to achieve greater strains. In general, it was found that moderate fields did not have the capability of producing large changes in volume fraction. Fig. 7 was typical of the several runs for this particular test and shows a change in strain of $\approx$0.5%. Using the present lattice parameters, this amounts to a relative change in volume fraction (variant one

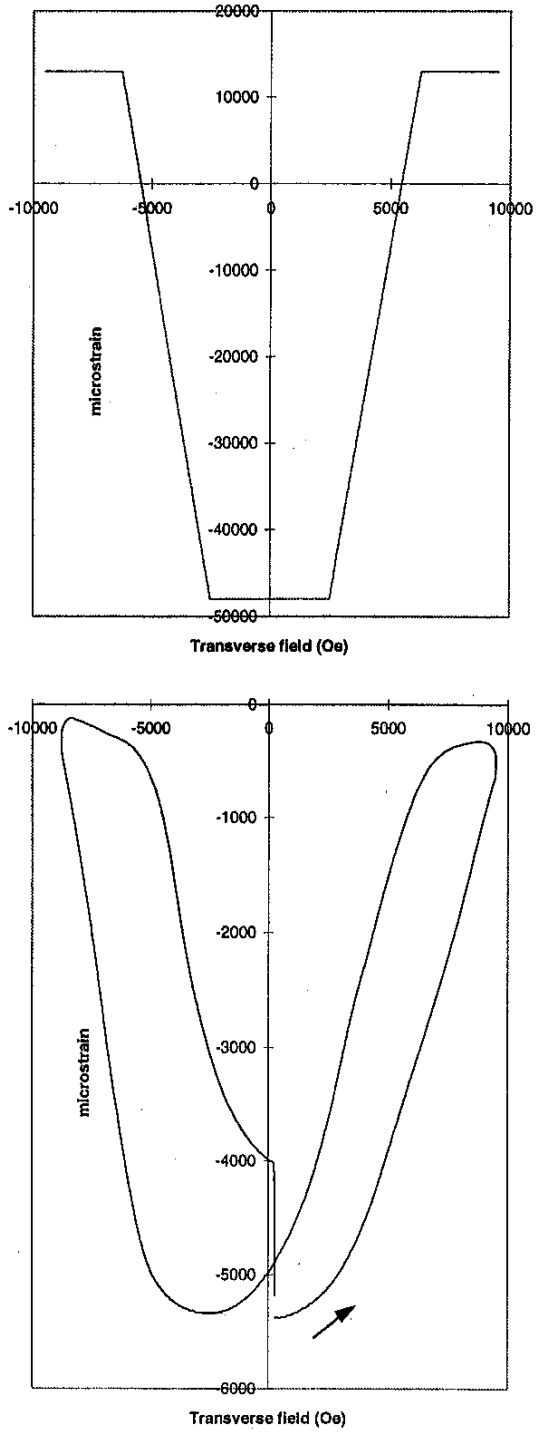

Fig. 7. Predicted and experimental curves for fixed axial, variable transverse field case. Arrow indicates start of test.

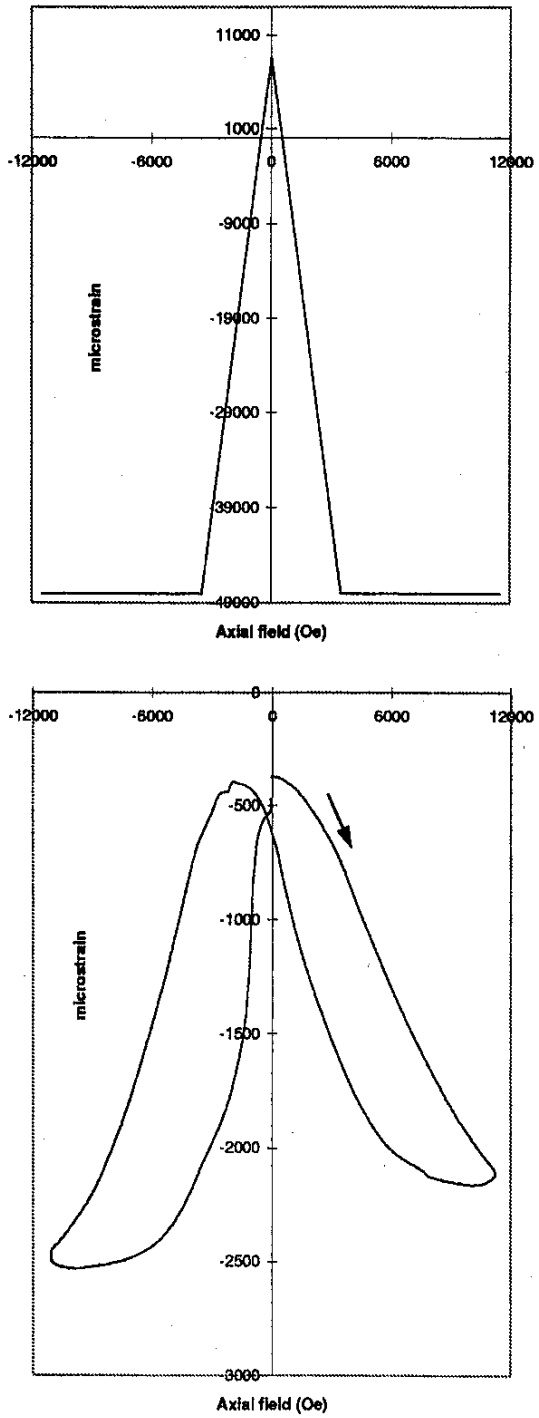

Fig. 8. Predicted and experimental curves for fixed transverse, variable axial field case. Arrow indicates start of test.

$\rightarrow$ variant two) of $\approx 8\%$. The slight microstructural changes observed optically during this test were consistent with this small volume fraction change.

B. Fixed Transverse Field, Variable Axial Field

For this experiment we fix $h_2 = c_2 = 3500$ Oe, and cycle the axial field h_1 about zero. This test corresponds to path B in Fig. 4(a), and Fig. 8 shows the predicted and experimental curves. Depending on the magnitude of c_2, the initial state ($h_1 = 0$) may be either single or multivariant. This is due to the fact that demagnetization energy competes with the transverse field to restrain it from saturating the magnetization in the short direction. In our case ($h_2 < 2\pi m_s$), the theory predicts a multivariant starting state at $h_1 = 0$. Fig. 5(b)

shows a possible series of compatible magnetoelastic domain structures corresponding to the predicted strain-field curve. In this sequence, the fixed transverse field favors variant two, but the initial state also contains variant one due to demagnetization effects. When the axial field reaches 4000 Oe, the specimen is completely transformed to variant one.

Experimentally, the curve agrees qualitatively with the theory, but the measured strains are again much smaller. Fig. 8 shows a variation of $\approx 0.2\%$ strain, which corresponds to a relative volume fraction change (variant two $\rightarrow$ variant one) of $\approx 3\%$. Very little microstructural change was observed during this test. The change in slope at the tails of the curve may indicate that saturation is beginning to occur in this case.

C. Fixed Axial Compression, Variable Transverse Field

Here we fix $\sigma = c_3 = 1.4$ or 4.2 MPa, and cycle transverse field h_2 about zero. This test corresponds to path C in Fig. 4(b). The theory assumes that any applied load will induce a single variant starting state consisting of variant E_1, i.e., any hindrances to twin boundary mobility are neglected so that an arbitrarily small stress will cause variant volume fractions to rearrange such that $\xi_1 = 1$. Experimentally, it was found that below a certain threshold load (usually around 2–3 MPa), large variant motion and strain was not induced, although a small amount did occur; for these cases, the discrepancy between theory and experiment was greater than tests with larger stresses. Fig. 9 was performed with 1.4 MPa compression, and was typical of these runs. Fig. 6 gives one possible set of compatible magnetoelastic domain structures corresponding to the predicted strain-field curve for 1.4 MPa compression. In this case there is nonuniqueness of the parameter η_1 as can be seen in Fig. 4(b); Fig. 6 shows one simple set of microstructures consistent with one solution, but there are many others. In particular, there are more complicated microstructures involving layers within layers, which allow an arbitrary volume fraction of 180 ° domains within variant one. In the sequence shown, the initial state consists of variant one biased by the axial compression with $\eta_1 = 0$. As the transverse field is applied, variant two is introduced, and at 6000 Oe the specimen is completely transformed to variant two. For increased loads, the material responds in usual shape-memory fashion with large jumps in strain. Fig. 10 shows the results of a 4.2 MPa compression test. The starting state had over 2% compression, and the test exhibited the largest hysteresis of all the runs.

Once again, while the shapes of the measured curves of strain versus field are similar to the predicted ones, the actual values of the strain are substantially smaller. It was observed, however, that the strains produced in runs with very small loads were larger than those obtained in the fixed field tests. With this in mind, we performed a test in which the specimen was first preloaded with 6 MPa compression. The load was then completely removed and the transverse field applied. This test produced the largest strain of all the runs, nearly 1.3%, as shown in Fig. 11. It also produced the most dramatic change in visible variant structure. Fig. 12 shows the microstructure present before and after the transverse field was applied.

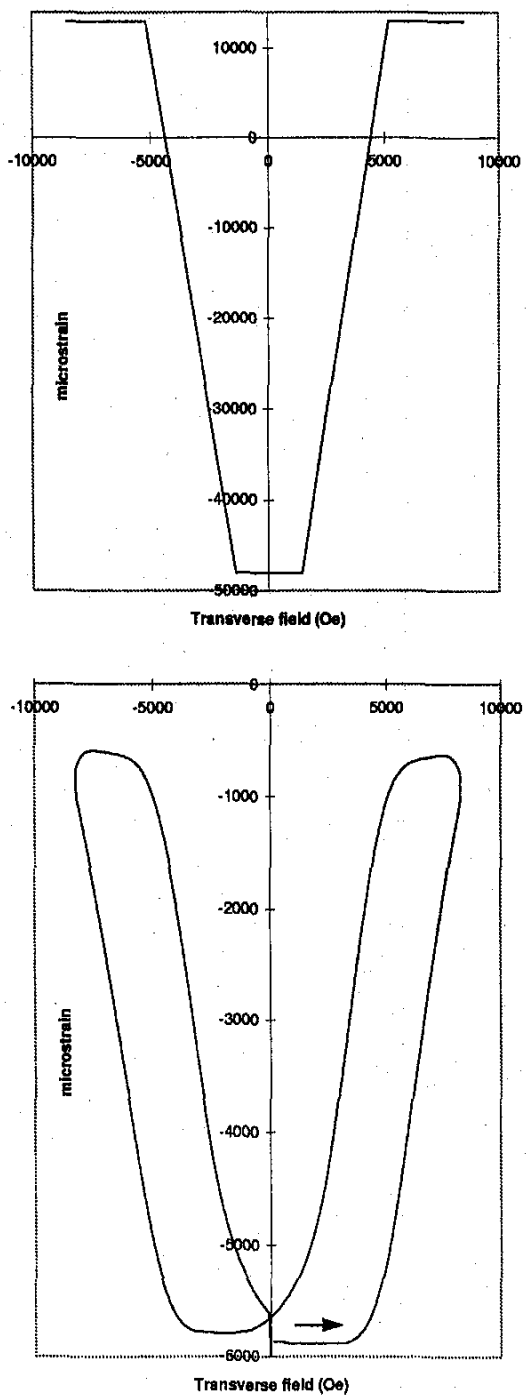

Fig. 9. Predicted and experimental curves for fixed 1.4 MPa axial load, variable transverse field case. Arrow indicates start of test.

We note that this change in microstructure agrees with the predicted magnetoelastic domain structures shown in Fig. 6. The results of this test emphasize the importance of the initial state of the material. This is discussed further below.

The results of the fixed axial compression tests can be used to make a preliminary evaluation of Ni_2MnGa's potential for actuator applications. One measure of work capacity considers

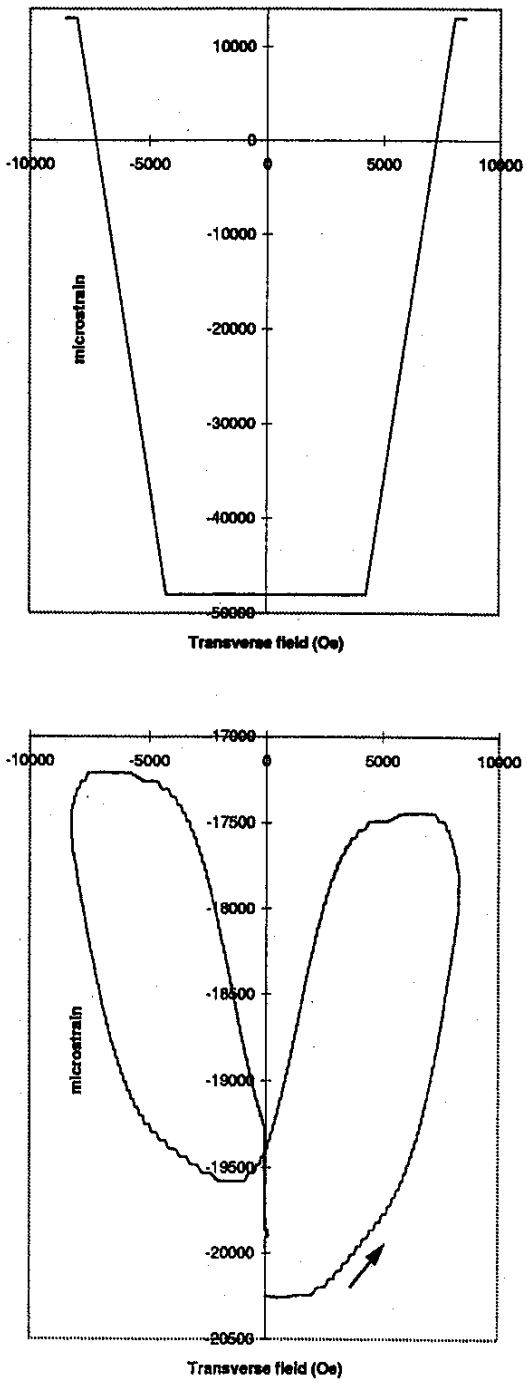

Fig. 10. Predicted and experimental curves for fixed 4.2 MPa axial load, variable transverse field case. Arrow indicates start of test.

the graph of applied load versus strain induced at maximum field. The fixed axial load tests give two data points: 5000 $\mu\epsilon$ at 1.4 MPa and 2750 $\mu\epsilon$ at 4.2 MPa. Assuming a linear trend, this implies a blocking stress of $\approx$7.6 MPa. For comparison, the magnetostrictive actuator material Terfenol can typically achieve 1800 $\mu\epsilon$ at 20 MPa and has a blocking stress of $\approx$60 MPa [11], [12]. The current data tentatively suggests that Ni_2MnGa might be useful for large stroke/small force

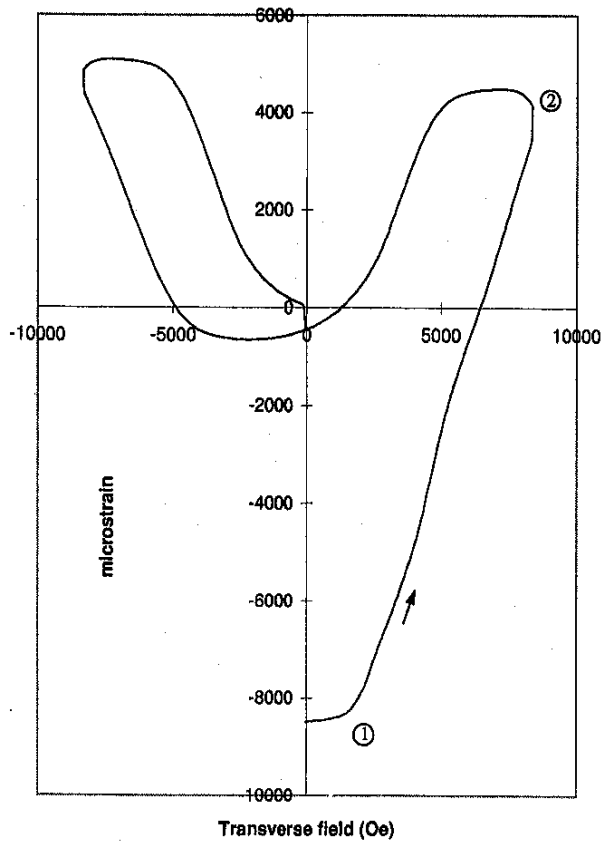

Fig. 11. Strain versus field results for transverse field applied after unloading from 6 MPa axial compression. Arrow indicates start of test.

applications. It should be noted that a more thorough study would consider additional specimen orientations and applied field directions.

We also note that rate effects related to twin boundary dynamics are present in these experiments. Fig. 13 compares two transverse field cycles done against 1.4 MPa axial compression. The field ramp rate was 150 Oe/s for the larger cycle and 300 Oe/s for the smaller. The curves suggest that twin boundary mobility plays a role in determining the total strain, and also contributes to larger hysteresis for the faster ramp rates. Relaxation effects can also be seen at the ends of the curves, where the strain slowly decreases in response to the applied load.

V. Discussion

In general, the experiments demonstrate how large strains can be achieved by using competing fields and loads. Strains of 1.3% have been observed for the best case of a suitably biased specimen in a transverse field test; the tests also tentatively suggest that the material has a work output capacity that might be useful for large strain/small force applications. Conceptually, the theory seems to capture the behavior of the material; the easy axes assumed for the variants appear to be correct, and the overall shape and symmetry of the curves agrees with experiment.

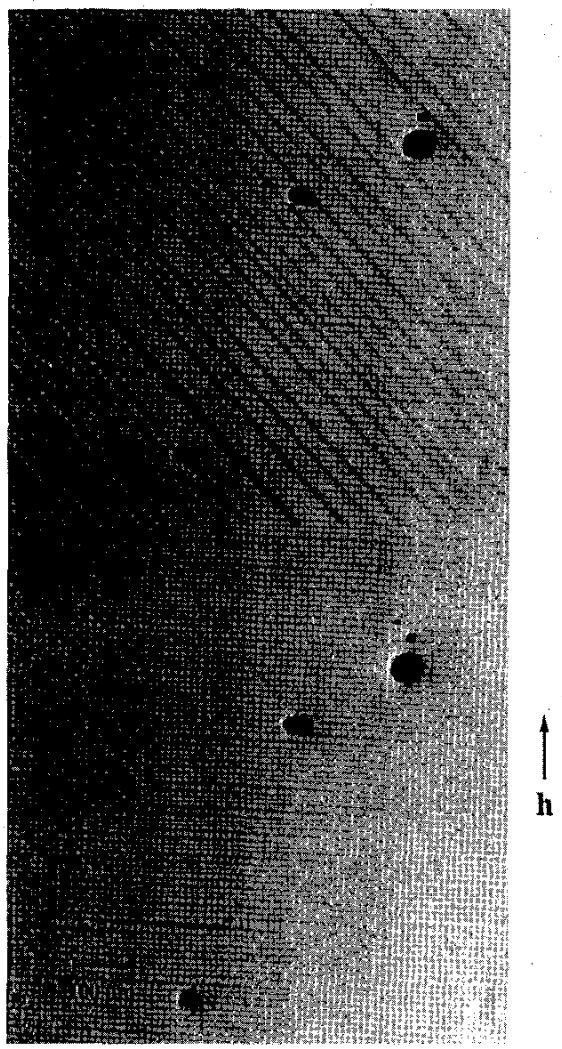

Fig. 12. (a) Observed microstructure after unloading from 6 MPa axial compression, 0 Oe (point 1 on Fig. 11. (b) After application of 10 000 Oe transverse field (point 2 on Fig. 11). Compare with schematic microstructures pictured in Fig. 6.

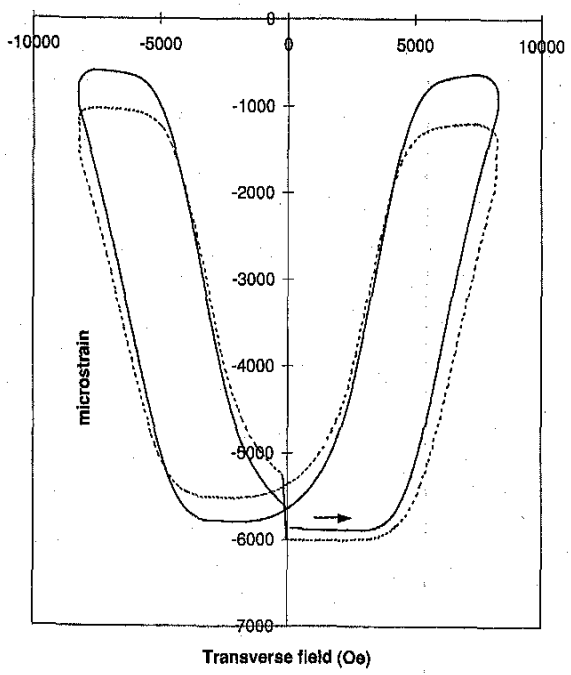

Fig. 13. Strain versus field with field ramp rates of 150 Oe/s (solid) and 300 Oe/s (dashed) for fixed 1.4 MPa axial load, variable transverse field case. Arrow indicates start of test.

A comparison of the present work with previous FePd [1] and NiMnGa [4] experiments reveals some important observations. The current results show that the Ni_2MnGa alloy exhibits significant hysteresis, approximately an order of magnitude larger strain hysteresis than that observed in $Fe_{70}Pd_{30}$; this is not accounted for by the energy minimization theory. This large hysteresis would need to be addressed in any potential actuator applications. In the experiments of Ullakko *et al.* [4], {110} and {100} fields were applied to a rectangular specimen resulting in strains of $\approx$600 $\mu\epsilon$ and $\approx$1300 $\mu\epsilon$, respectively. These smaller strains may be explained by the fact that no competing bias field or stress was used in these tests.

An analysis of the present results and those of Ullakko *et al.* also raises the issue of the best field orientation for producing a large field-induced change of shape in a twinned single crystal of Ni_2MnGa or related alloy. One possible strategy is to apply the field in a direction that maximizes the driving force on a twin boundary in the sense of Eshelby, i.e., the rate of change in energy per unit displacement of the boundary. Consider a series of parallel twin bands consisting of two variants of martensite having alternating magnetizations $\mathbf{m}_1, \mathbf{m}_2, \mathbf{m}_1, \mathbf{m}_2, \ldots$ (e.g., Fig. 5(a), 5000 Oe). If only the applied field energy is considered, then the driving force on a twin boundary is proportional to $\mathbf{h} \cdot (\mathbf{m}_1 - \mathbf{m}_2)$. If we maximize this driving force over all directions of the applied field $\mathbf{h}$, keeping its magnitude fixed, and use the easy axes of Ni_2MnGa, we find that the driving force is maximized in the {110} direction parallel to $\mathbf{m}_2 - \mathbf{m}_1$. Energy minimization, however, gives a contrary result: it implies that a field applied along this direction favors the two variants equally. The reason for the discrepancy is that the energy minimizer with a {110} applied field can be more complicated than the assumed simple picture of alternating magnetizations. That is, it generally exhibits 180° domains within each martensite band or the presence of the third variant. Thus, energy minimization implies that a field applied in one of the easy directions strongly favors one variant over another.

Taken together, the available experimental results in the NiMnGa and FePd systems show a consistent qualitative agreement with theory, but a consistent overestimation of the theoretically predicted macroscopic strains. There are several possible explanations for this; we first consider the issue of variant nucleation. The theory assumes that the applied fields can nucleate variants as necessary to achieve minimum energy. Direct observation of microstructural changes (Fig. 12) indicate that applied fields move only variant interfaces that are already present. With sufficient field energy, one could

imagine nucleation of a favorable variant might occur, but this process competes with the rotation of the magnetization in the variant present. This raises the issue of the starting state of the experiment. If nucleation presents a large energy barrier, it might be necessary to bias a specific initial microstructure (using a stress or field) that is favorable to achieving strains without requiring nucleation. The preload test described above (Fig. 11) is an example of this biasing strategy.

The experimental graphs also show significant hysteresis, which cannot of course be predicted by absolute energy minimization. A theory of hysteresis based on relative energy minimization (i.e., minimization with respect to localized but large amplitude disturbances) was proposed by Ball *et al.* [13]. This theory can be adapted to the present situation and appears to be consistent with the differences in the size of hysteresis among the three experiments shown here and that observed in $Fe_{70}Pd_{30}$.

Apart from nucleation issues, magnetization rotation is the most likely explanation for the discrepancy between theory and experiment. The theory assumes that each variant has a fixed magnetization and that the energy due to an applied field is minimized by either nucleating favorable variants or increasing the volume fraction of favorable variants present through twin boundary movement. In practice, there is an energy barrier associated with both nucleation and interface mobility, and it is possible that in some cases it is more favorable for the magnetization in a particular variant to rotate in order to reduce energy. To quantify this, it is necessary to determine the anisotropy constants for a single variant of the martensite. An important related quantity is the measurement of the magnetostriction constants for a single variant, for if this rotation occurs, the associated strain is likely to be incompatible with that in the neighboring twin bands, giving an effective restoring force that would tend to prevent magnetization rotation. Recent experiments [14] by the authors have measured both these quantities in the single variant state for Ni_2MnGa. The results indicate that while the anisotropy constant is large enough ($\sim 10^6$ ergs/cm^3) to promote the ferromagnetic shape memory effect, it is also consistent with calculations predicting the relatively small blocking stress values seen in the experiments (see [14] for details). These quantities will allow for improvements to the present theory to include the effects of magnetization rotation.

Finally, the rate effects noted in Section IV-C also constrain the amount of induced strain. These effects, as well as the hysteretic effects mentioned above, would need to be addressed in high frequency/large strain actuator applications.

ACKNOWLEDGMENT

The authors would like to thank A. DeSimone for comments on a first draft of this paper.

REFERENCES

[1] R. D. James and M. Wuttig, "Magnetostriction of martensite," *Phil. Mag. A*, vol. 77, no. 5, pp. 1273–1299, 1998.

[2] ——, "Mathematics and control in smart structures," in *Proc. SPIE Symp. Smart Structures .Materials*, V.V. Varadan and J. Chandra, Eds., 1996, vol. 2715, p. 420.

[3] A. DeSimone and R. D. James, *A Constrained Theory of Magnetoelasticity*, preprint.

[4] K. Ullakko, J. K. Huang, C. Kantner, R. C. O'Handley, and V. V. Kokorin, "Large magnetic-field-induced strains in NMG single crystals," *Appl. Phys. Lett.*, vol. 69, pp. 1966–1968, 1996.

[5] R. C. O'Handley, "Model for strain and magnetization in magnetic shape-memory alloys," *J. Appl. Phys.*, vol. 83, pp. 3263–3270, 1998.

[6] A. DeSimone and R. D. James, "A theory of magnetostriction oriented towards applications," *J. Appl. Phys.*, vol. 81, pp. 5706–5708, 1997.

[7] L. D. Landau, E. M. Lifshitz, and L. P. Pitaevskiĭ, *Electrodynamics of Continuous Media*, 2nd ed. New York: Pergamon, 1984.

[8] W. F. Brown, "Magnetoelastic interactions," in *Springer Tracts in Natural Philosophy*. New York: Springer-Verlag, 1966, vol. 9.

[9] I. K. Zasimchuk, V. V. Kokorin, V. V. Martynov, A. V. Tkachenko, and V. A. Chernenko, "Crystal structure of martensite in Heusler alloy NMG," *Phys. Met. Metall.*, vol. 69, no. 6, pp. 104–108, 1990.

[10] A. DeSimone, "Energy minimizers for large ferromagnetic bodies," *Arch. Rational Mech. Anal.*, vol. 125, pp. 99–143, 1993.

[11] A. E. Clark, J. P. Teter, and O. D. McMasters, "Magnetostriction "jumps" in twinned $Tb_{0.3}Dy_{0.7}Fe_{1.9}$," *J. Appl. Phys.*, vol. 63, pp. 3910–3912, 1988.

[12] D. C. Jiles, "The development of highly magnetostrictive rare earth-iron alloys," *J. Phys. D, Appl. Phys.*, vol. 27, pp. 1–11, 1994.

[13] J. M. Ball, C. Chu and R. D. James, "Hysteresis during stress-induced variant rearrangement," *J. Phys. IV, Colloque C8*, vol. 5, pp. 245–251, 1995.

[14] R. Tickle and R. D. James, "Magnetic and magnetomechanical properties of NMG," *J. Magnetism Magn. Mater.*, vol. 195, pp. 627–638, 1999.